

# State-dependent parameter model identification for inverse dead-zone control of a hydraulic manipulator<sup>\*</sup>

C. West<sup>\*</sup> E. D. Wilson<sup>\*</sup> Q. Clairon<sup>\*\*</sup> S. Monk<sup>\*</sup>  
A. Montazeri<sup>\*</sup> C. J. Taylor<sup>\*</sup>

<sup>\*</sup> *Engineering Department, Lancaster University, UK*  
(*e-mail: c.west@lancaster.ac.uk, e.d.wilson1@lancaster.ac.uk,*  
*s.monk@lancaster.ac.uk, a.montazeri@lancaster.ac.uk,*  
*c.taylor@lancaster.ac.uk*)

<sup>\*\*</sup> *School of Mathematics and Statistics, University of Newcastle, UK*  
(*e-mail: Quentin.Clairon@ncl.ac.uk*)

---

**Abstract:** The robotic platform in this study has dual, seven-function, hydraulically actuated manipulators, which are being used for research into assisted tele-operation for common nuclear decommissioning tasks, such as pipe cutting. The article concerns the identification of state-dependent parameter (SDP) models for joint angle control. Compared to earlier SDP analysis of the same device, the present work proposes a new way of representing the state-dependent gain and parametrises this using novel regret-regression methods. A mechanistic interpretation of this model yields dead-zone and angular velocity saturation coefficients, and facilitates SDP-based control with an inverse dead-zone. This approach integrates the input signal calibration, system identification and nonlinear control system design steps, using a relatively small dataset, allowing for straightforward recalibration when the dynamic characteristics have changed due to age and use, or after the installation of replacement parts.

*Keywords:* Identification for control; nonlinear system identification; parameter-varying systems; robotic manipulators; anti-windup; application of nonlinear analysis and design

---

## 1. INTRODUCTION

The research behind this article concerns the development of autonomous and assisted tele-operated robotic systems for the nuclear industry. The mobile platform used for the experimental work has dual, seven-function, hydraulically actuated manipulators (Taylor and Robertson, 2013; Montazeri et al., 2017), for which the authors are investigating use of vision-based interfaces for common nuclear decommissioning tasks, such as pipe cutting. Marturi et al. (2016), for example, discuss some of the challenges involved and the results of a related pilot study. It is clear that, to improve safety, task execution speed and operator training-time for certain tasks, high performance control of the nonlinear manipulator dynamics is required, necessitating the identification of suitable models.

Conventional identification methods for robotic systems include maximum likelihood (Olsen et al., 2001), the extended Kalman filter (Gautier and Poignet, 2001), inverse dynamic identification model with least squares (IDIM-LS; Gautier et al. 2013) and frequency domain methods (Wernholt and Gunnarsson, 2008), among oth-

ers. Instrumental variable and Refined Instrumental Variable (RIV) algorithms have also been used for modelling robotic systems, sometimes in combination with State-Dependent Parameter (SDP; Taylor and Robertson 2013) and inverse dynamic models (Janot et al., 2014).

SDP models are estimated from data within a stochastic state-space framework (Young, 2011) and take a similar structural form to linear parameter-varying systems (Hashemi et al., 2012), with both based on the definition of quasi-linear forms. The parameters of SDP models are functionally dependent on measured variables, such as joint angles and velocities in the case of manipulators. Such models have been identified and successfully used for SDP control of a KOMATSU hydraulic excavator (Taylor et al., 2007b) and a BROKK-HYDROLEK device (Taylor and Robertson, 2013). The recent article by Janot et al. (2017) further demonstrates the advantages of the SDP approach, in comparison to IDIM-LS methods, when applied to an electro-mechanical positioning system and a TX40 robot.

In comparison to a typical machine driven by electric motors, hydraulic actuators generally have higher loop gains, wider bandwidths and lightly-damped, nonlinear dynamics (e.g. Sirouspour and Salcudean, 2001). For the BROKK-based nuclear decommissioning platform alluded to above, these dynamics have been represented using physically-based (mechanistic) equations (e.g. Montazeri et al., 2017). However, the present article instead focuses

---

<sup>\*</sup> This work is supported by the Engineering and Physical Sciences Research Council (EPSRC), EP/M015637/1 and EP/R02572X/1. The authors are also grateful for the support of the Nuclear Decommissioning Authority. The modelling algorithms are available as the CAPTAIN Toolbox (Taylor et al., 2007a), which may be freely downloaded from: <http://www.lancaster.ac.uk/staff/taylorcj/tdc>.

### 3. METHODOLOGY

on the identification from data of a relatively straightforward SDP model form, which is directly used for nonlinear control design. In contrast to earlier SDP modelling results for the same device (Robertson et al., 2012; Taylor and Robertson, 2013), the present work investigates the angular velocity of each joint. This yields a new SDP model structure that better highlights the asymmetric actuation, and provides implicit estimates of the dead-zone and angular velocity saturation, in a similar manner to the friction analysis of Janot et al. (2017).

Uniquely, recent results linking regret-regression statistical estimation (Henderson et al., 2010) with state-space models (Clairon et al., 2017), are investigated for the final, parametric stage of the SDP analysis. Finally, the SDP models obtained in this manner facilitate use of a straightforward, Inverse Dead-Zone (IDZ; e.g. Fortgang et al. 2002) method for control system design, combined with either conventional PI or Proportional-Integral-Plus (PIP) methods (Taylor et al., 2013). Whilst system identification is the main focus of this article, closed-loop control performance is briefly investigated, using both the identified SDP model and laboratory experiments. Section 2 of the article briefly introduces the robotic platform, while section 3 describes the system identification methodology. This is followed by the modelling and control results in sections 4 through to 6, and the conclusions in section 7.

### 2. ROBOTIC PLATFORM

Two hydraulically actuated HYDROLEK-7W manipulators, each with seven degrees of freedom have been attached to a BROKK-40 mobile platform, and developed at Lancaster University for research into the decommissioning, repairs and maintenance of nuclear power plants (see images here: <https://tinyurl.com/yd3bvsl0>). The movements of the manipulator joints are controlled using National Instrument (NI) tools. Hence, in the following, the controlled output  $y_k$  is a calibrated potentiometer signal representing a specified joint angle, in degrees, while the input  $v_k$  lies in the range  $\pm 10V$ , where the sign indicates the required direction of movement. In practical terms, a different valve is used for increasing or decreasing the angle of each joint, hence a voltage in the range 0 to 10 is applied to the appropriate valve via the NI Compact Field Point (NI-CFP) computer.

The present authors are researching the use of assisted tele-operation to reduce cognitive workload. This is briefly described by West et al. (2017), with more detailed articles in preparation. Preliminary work has focused on pipe cutting as an illustration of the generic approach, since this is a common repetitive task in nuclear decommissioning. The user selects the object to be cut from an on-screen image, whilst the computer control system determines the required position and orientation of the manipulators in 3D space, and calculates the necessary joint angles for the manipulator to grasp and cut. This approach has similarities to recent work by Marturi et al. (2016) and Kent et al. (2017). However, testing for realistic tasks, even in a laboratory environment, has identified the need for improved hydraulic control systems to provide more accurate movement of the manipulators, motivating the research discussed below.

Consider the deterministic form of the SDP model:

$$y_k = \mathbf{w}_k^T \mathbf{p}_k \quad (1)$$

where  $\mathbf{w}_k^T$  is a vector of lagged input and output variables and  $\mathbf{p}_k$  is a vector of SDP parameters, defined as follows,

$$\mathbf{w}_k^T = [-y_{k-1} \quad -y_{k-2} \quad \cdots \quad -y_{k-n} \quad v_{k-1} \quad \cdots \quad v_{k-m}]$$

$$\mathbf{p}_k = [a_1 \{\chi_k\} \quad \cdots \quad a_n \{\chi_k\} \quad b_1 \{\chi_k\} \quad \cdots \quad b_m \{\chi_k\}]^T$$

Here  $v_k$  and  $y_k$  are the input and output signals respectively, while  $a_i \{\chi_k\}$  and  $b_j \{\chi_k\}$  are  $n$  and  $m$  state dependent parameters. The latter are assumed to be functions of a non-minimal state vector  $\chi_k$ , the elements of which are measured variables. In the simplest case,  $\chi_k = \mathbf{w}_k$ . Time-delays  $\tau \geq 1$  are represented by setting  $b_1 \{\chi_k\} = \cdots = b_{\tau-1} \{\chi_k\} = 0$ . Following e.g. Young (2011), the SDP model is usually identified in three stages, as follows.

**Step 1.** The underlying model structure and potential state variables are first identified by RIV estimation of discrete-time linear transfer function models (Taylor and Robertson, 2013). In this regard, open-loop step experiments using the manipulator suggest that a first order linear difference equation, i.e.,

$$y_k = -a_1 y_{k-1} + b_\tau v_{k-\tau} \quad (2)$$

provides an approximate representation of individual joints, with time-invariant parameters  $\{a_1, b_\tau\}$  and the time delay  $\tau$  depending on the sampling interval  $\Delta t$ .

**Step 2.** It is readily apparent that the values of  $\{a_1, b_\tau\}$  are not repeatable for experiments with step inputs of different magnitudes. Furthermore, the model performs poorly for experiments based on inputs with time-varying magnitudes (see later Table 2 and Fig. 4). Hence, to determine the state-dependent form of these parameters, the second stage of SDP analysis usually involves the estimation of a related time-varying parameter model, embedded within a data reordering and back-fitting algorithm (Taylor et al., 2007a). In this regard, SDP analysis of experimental data suggests that  $a_1 = -1$  is time invariant (a similar result is obtained by Janot et al. 2017), whilst the SDP  $b_\tau \{\chi_k\} = b_\tau \{v_{k-\tau}\}$  is a static nonlinear function of the delayed input signal. In other words, the model is an integrator with nonlinear gain and time-delays.

However, prior articles concerning these manipulators (e.g. Robertson et al., 2012; Taylor and Robertson, 2013) have all utilised a scaled input signal designed to eliminate dead-zone nonlinearities in an *ad hoc* manner (since this is the approach taken for the original industry control system). This rather time-consuming calibration needs repeating from time to time as the hardware is serviced and maintained. By contrast, the present article develops a more systematic approach, in which the dead-zone estimation is encompassed within the SDP model, while steps 1 and 2 are blended into a single identification stage, all based on RIV estimation of the linear model (2) without back-fitting, as discussed in the following section 4.

**Step 3.** In the final, optimization stage,  $b_\tau \{v_{k-\tau}\}$  is parameterized in some manner i.e. expressed as a function of the dependent variable  $v_k$ . The coefficients of this model are estimated directly from data  $(v_k, y_k)$  using some form

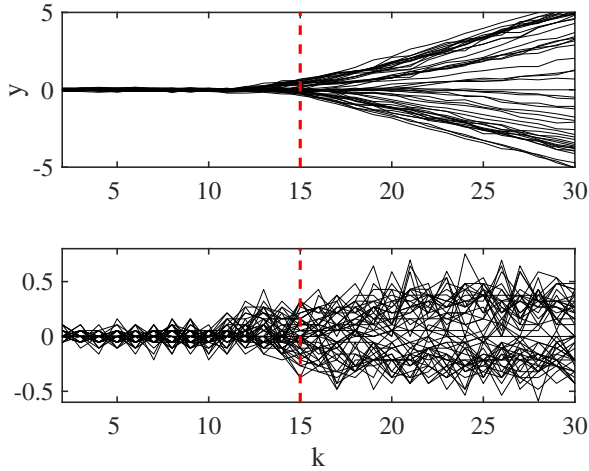


Fig. 1. Joint angle  $y_k$  (upper subplot) and differenced angle  $y_k - y_{k-1}$  (lower), plotted against sample  $k$  for 40 experiments, each based on a step input at  $k = 0$  of varying magnitudes, with  $\Delta t = 0.01$ s. The estimated time-delay  $\tau = 15$  samples is also shown (dashed).

of nonlinear optimisation. The present article considers novel regret-regression methods (Henderson et al., 2010) for this purpose. Developed for applications in medical statistics, regret-regression has particular value when the signals are highly noisy and the data set consists of numerous, relatively short experiments. This appears apt in the case of angular velocities derived (without smoothing) from the open-loop experiments shown in Fig. 1. Recent research links regret-regression methods with state-space modelling (Clairon et al., 2017), hence the method can be utilised in the present context for system identification.

#### 4. SYSTEM IDENTIFICATION

The upper subplot of Fig. 1 illustrates typical open-loop step response data for one of the manipulator joints, namely the right hand side shoulder joint, denoted J2 below, normalised for initial conditions of zero. Using the raw data sampling rate  $\Delta t = 0.01$ s, with  $a_1 = -1$  and  $\tau = 15$  determined *a priori* as discussed above, RIV estimates  $b_\tau$  for each experiment are shown in Fig. 2, demonstrating the clear state-dependency on the input.

The mechanistic interpretation of this emergent state-dependency is straightforward: using equation (2) with  $a_1 = -1$  yields  $b_\tau v_{k-\tau} = y_k - y_{k-1}$  i.e.  $b_\tau v_{k-\tau}$  represents a smoothed estimate of the differenced sampled output signal and  $b_\tau v_{k-\tau}/\Delta t$ , as plotted in Fig. 3, provides an estimate of the angular velocity in degrees/s. This interpretation of the model highlights the dead-zone and velocity saturation limits i.e. any inputs to the NI-CFP computer in the range  $-1.33 < v_k < 1.31$  (for this particular joint) are insufficient to overcome the hydraulic system design and friction effects, while the angular velocity saturates for  $|v_k|$  greater than  $\approx 5$ V.

Since this hydraulic system has just one, physically meaningful, state-dependent parameter, the back-fitting algorithm alluded to above, in Step 2, is not required. Exponential functions could be directly fitted to the RIV estimates in Fig. 3. Two functions are required for each joint because there is asymmetrical actuation e.g. the saturation

velocities for J2 are  $-29.5$  and  $38.9$  degrees/s. However, since this approach yields promising results (details are omitted for brevity), it makes sense to move immediately to optimisation of the identified SDP model structure in affine form (Step 3). Here, denoting  $q\{v_k\} = b_\tau\{v_k\} \times v_k$ , the model is conveniently expressed as follows,

$$y_k = y_{k-1} + q\{v_{k-\tau}\} \quad (3)$$

with,

$$y_k = y_{\min} \text{ for } y_k < y_{\min} ; y_k = y_{\max} \text{ for } y_k > y_{\max} \quad (4)$$

where  $y_{\min}$  and  $y_{\max}$  are the hardware limits and,

$$\begin{aligned} q\{v_k\} &= (1 - \alpha_1) e^{\alpha_2(\alpha_3 - v_k)} \text{ for } v_k < \alpha_3 \\ q\{v_k\} &= 0 \text{ for } \alpha_3 \leq v_k \leq \alpha_6 \\ q\{v_k\} &= (1 - \alpha_4) e^{\alpha_5(v_k - \alpha_6)} \text{ for } v_k > \alpha_6 \end{aligned} \quad (5)$$

For J2,  $y_{\min} = -13.8^\circ$  and  $y_{\max} = 63.6^\circ$ , while the coefficients for the static nonlinearity in Fig. 3 are estimated directly from the step response data  $(y(k), v(k))$  in Fig. 1 as follows:  $\hat{\alpha}_1 = -0.2951$ ,  $\hat{\alpha}_2 = 1.3560$ ,  $\hat{\alpha}_3 = -1.3298$ ,  $\hat{\alpha}_4 = 0.3887$ ,  $\hat{\alpha}_5 = 1.7710$  and  $\hat{\alpha}_6 = 1.3124$ . Here, for each input sequence, the data illustrated in the upper subplot of Fig. 1 are compared with the model response obtained using equations (3) to (5), the sum of the least squares output (simulation) errors are determined, and the mean of these errors over the entire data set is used as the objective function for `fminsearch` in MATLAB. Where the local minimum was unchanging, regardless of the initial conditions, we used this as the minimum. Although this does not guarantee a global minimum, the method yields good results for the particular examples considered below.

Note  $(\alpha_2, \alpha_5)$  are curve coefficients;  $\alpha_1/\Delta t = -29.5^\circ/s$  and  $\alpha_4/\Delta t = 38.9^\circ/s$  provide estimates of the minimum and maximum angular velocity saturation limits; and  $\alpha_3 = -1.33$ V and  $\alpha_6 = 1.31$ V represent the values of  $v_k$  between which the manipulator does not move i.e. the dead-zone. These objective estimates compare closely with equivalent values obtained from extensive *ad hoc* experimental work. In this regard, although Fig. 3 shows the estimated angular velocity, it should be stressed that the model coefficients are based on `fminsearch` estimation of the SDP model using the raw data  $(v_k, y_k)$  i.e. the joint angles from the upper subplot of Fig. 1. The SDP model can also be optimised directly using a smaller number of experiments based on a random sequence of input magnitudes, similar to Fig. 4 discussed below, and this yields similar results. The relative merits of this novel approach to estimating the velocity are being investigated by the authors.

Although the coefficients  $\alpha_i$  in (5) can be satisfactorily estimated using standard MATLAB tools, the present authors are also investigating the use of regret-regression methods (Henderson et al., 2010). In this regard, Table 1 utilises the above SDP model as a simulation tool, in which the length of the simulated time series and the level of noise can be adjusted, in order to investigate the relative performance of different optimisation algorithms. In the particular case shown, based on 100 experiments of 10 samples each, and with the state and noise variance both  $\sigma^2 = 0.001$ , the `fminsearch` and regret estimates of the static nonlinearity are very similar. However, further research is required for different input and noise scenarios.

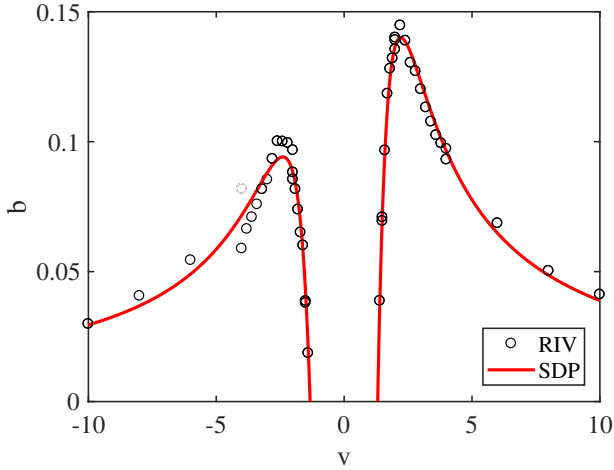


Fig. 2. State-dependent parameter plotted against input magnitude (i.e. steady state voltage to NI-CFP,  $v_\infty$ ), showing RIV estimates  $b_\tau$  for individual step experiments (circles) and optimised SDP  $b_\tau \{\chi_k\}$  (solid).

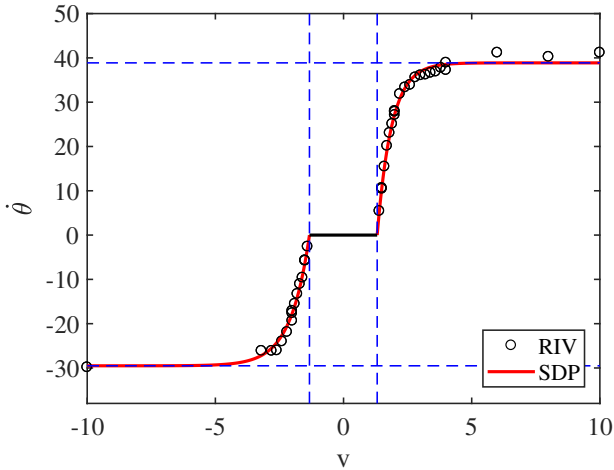


Fig. 3. Angular velocity  $\dot{\theta}$  (degrees/s) plotted against input magnitude (i.e. steady state voltage to NI-CFP,  $v_\infty$ ), showing RIV estimates  $b_\tau \times v_\infty / \Delta t$  for individual step experiments (circles) and SDP  $b_\tau \{\chi_k\} \times v_\infty / \Delta t$  (solid trace). The estimated dead-zone and angular velocity saturations are also shown (dashed).

## 5. MODEL EVALUATION

Fig. 4 shows an illustrative model evaluation experiment, based on the regret-regression estimates of the SDP model (3) to (5), while Table 2 shows the mean absolute error (MAE) of the model for this (first row) and eight additional experiments. Here, each experiment takes a similar form to Fig. 4 but with randomly generated input sequences. The experimental data in Fig. 4 and Table 2 are for the BROKK manipulator in the laboratory. The SDP model adequately represents the joint angle system dynamics for basic simulation purposes and, as discussed later, control system design. In fact, Table 2 compares the SDP model with two benchmark models and yields considerably improved performance in both cases. The other models include a simplified dead-zone model based

Table 1. Optimised coefficients  $\alpha_i$  ( $i = 1 \dots 6$ ) for simulated data. SDP refers to the coefficients used in the simulation (the ‘true’ values), RR are the regret-regression estimates and FM are the `fminsearch` estimates.

	$\alpha_1$	$\alpha_2$	$\alpha_3$	$\alpha_4$	$\alpha_5$	$\alpha_6$
SDP	2.2161	1.3570	-1.3266	2.9315	1.7865	1.3149
RR	2.2163	1.3562	-1.3265	2.9315	1.7873	1.3151
FM	2.2126	1.3694	-1.3277	2.9308	1.7873	1.3139

Table 2. Evaluation experiments, showing the mean absolute error between the output response of the model and measured data from the BROKK for: the SDP model based on equations (3)-(5); a simplified SDP dead-zone (DZ) model based on equations (3), (4) and (6); and the linear model (2).

Experiment	SDP	SDP-DZ	Linear
1	4.71	7.52	16.26
2	6.14	9.51	22.43
3	3.02	6.26	44.78
4	2.75	6.77	38.48
5	2.25	6.52	40.32
6	2.76	6.21	42.65
7	4.38	18.26	15.56
8	10.37	16.91	35.20
9	5.00	9.94	44.25

on equations (3), (4) and (6); and the linear model (2). The linear model is individually optimised for each data set (otherwise the results are even poorer than indicated in Table 2), whilst both SDP models are estimated *a priori* as discussed above. Finally, similar SDP model forms are identified for the other joints of both manipulators. In the case of Joints 1–3 (azimuth yaw, shoulder pitch and elbow pitch), these yield satisfactory model evaluation results, including for open-loop experiments involving simultaneous movement of several joints and for resolved motion. However, the two joints closest to the end-effector (Joints 4–5: the forearm roll and wrist pitch), yield inconsistencies in the system time-delay and poorer results, and this is the subject of on-going research by the authors.

## 6. CONTROL DESIGN

Fig. 5 shows a schematic representation of the proposed control system. In the discrete-time case,  $d_k$  is the desired joint angle,  $u_k$  is the PI or PIP control input variable,  $v_k$  is the voltage to the NI-CPF computer in the range  $\pm 10V$ ,  $q_k$  is the angular velocity and  $y_k$  is the joint angle. The SDP model identified above, i.e. equations (3) to (5), describes the relationship between  $v_k$  and  $y_k$ . In order to investigate closed-loop robustness, the coefficients  $\hat{\alpha}_i$  ( $i = 1 \dots 6$ ) used for control design may take different values to those of the SDP simulation model developed above.

Whilst previous research into nonlinear control of this device has directly utilised the SDP model in a special form of pole assignment (Taylor et al., 2011; Taylor and Robertson, 2013), the present article investigates a rather simpler IDZ approach. This is based on an approximation of Fig. 3 close to the dead-zone limits, as illustrated by Fig. 6. A control sampling rate of  $\Delta t = 0.05s$  is chosen

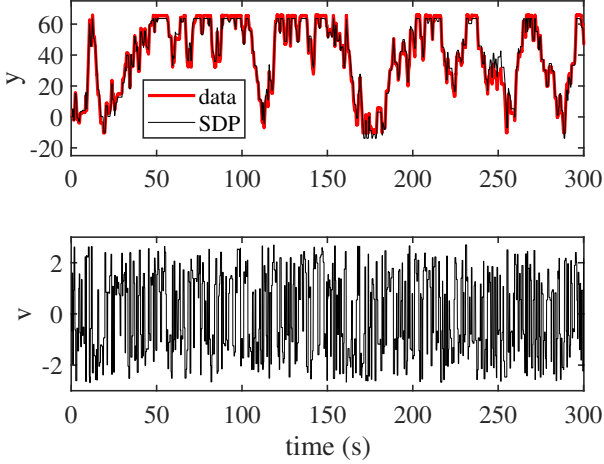


Fig. 4. SDP model evaluation, showing the joint angle  $y_k$  (upper subplot) and input  $v_k$  (lower) plotted against time (s). The upper subplot compares the model response (thin trace) with experimental data (thick).

as a compromise between satisfactory reaction times and a relatively low order PIP control system. In this case, Fig. 6 shows the linearised relationships for  $v_k$  and  $q_k$  in the range (i)  $v_{\min}$  to  $\hat{\alpha}_3$  and (ii)  $\hat{\alpha}_6$  to  $v_{\max}$  in the negative and positive directions of movement, respectively. For J2,  $v_{\min} = -2.2$  and  $v_{\max} = 1.75$  are chosen by trial and error to obtain a satisfactory closed-loop response in simulation; these input values are equivalent to an angular velocity  $\approx 20^\circ/\text{s}$  in either direction, and it seems unlikely that any faster movement would be desirable in practice.

This approximation of the SNL element of Fig. 5 is defined as follows (cf. equations (5)):

$$\begin{aligned} q\{v_k\} &= s_n(v_k - \hat{\alpha}_3) \quad \text{for } v_k < \hat{\alpha}_3 \\ q\{v_k\} &= 0 \quad \text{for } \hat{\alpha}_3 \leq v_k \leq \hat{\alpha}_6 \\ q\{v_k\} &= s_p(v_k - \hat{\alpha}_6) \quad \text{for } v_k > \hat{\alpha}_6 \end{aligned} \quad (6)$$

where the ‘slope’ coefficients associated with negative and positive inputs are  $s_n = q\{v_{\min}\}/(v_{\min} - \hat{\alpha}_3)$  and  $s_p = q\{v_{\max}\}/(v_{\max} - \hat{\alpha}_6)$ , respectively. Adapting e.g. Fortgang et al. (2002), the IDZ control element is,

$$\begin{aligned} v_k &= u_k/s_n + \hat{\alpha}_3 \quad \text{for } u_k < -\beta \\ v_k &= 0 \quad \text{for } -\beta \leq u_k \leq \beta \\ v_k &= u_k/s_p + \hat{\alpha}_6 \quad \text{for } u_k > \beta \end{aligned} \quad (7)$$

where  $\beta = 0.05$  (for the laboratory experiments below) is a ‘chatter’ coefficient, introduced to avoid unnecessary switching of the input between  $\hat{\alpha}_3$  and  $\hat{\alpha}_6$ . Here, equations (7) aim to cancel the system dead-zone and allow use of conventional linear control design methods to address any remaining dynamics and time-delays. For J2,  $\tau = 3$  and hence, using standard methods (Taylor et al., 2013), based on the linear model (2) with  $b_3 = -a_1 = 1$ , the PIP control algorithm takes the following incremental form,

$$\begin{aligned} u_k &= u_{k-1} - g_1(u_{k-1} - u_{k-2}) - g_2(u_{k-2} - u_{k-3}) \\ &\quad - f_0(y_k - y_{k-1}) + k_I(d_k - y_k) \end{aligned} \quad (8)$$

where  $u_k = u_{\min}$  for  $u_k < u_{\min}$ ,  $u_k = u_{\max}$  for  $u_k > u_{\max}$ , in which  $u_{\min} = -2.5$  and  $u_{\max} = 2.5$  are introduced

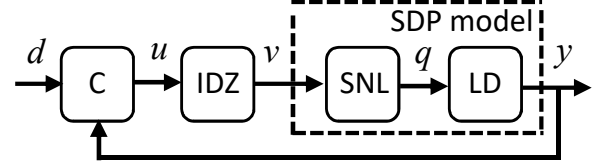


Fig. 5. Schematic diagram of the control system, in which C, IDZ, SNL and LD represent the (linear) Controller, Inverse Dead-Zone control element, Static NonLinearity and Linear Dynamics, respectively.

to avoid potential integral-wind up problems. There are several options for selecting these control input limits. The signals to the NI-CFP computer are limited to  $\pm 10\text{V}$  but Fig. 3 shows that, in practical terms, the angular velocity already saturates for input signals greater than  $\approx \pm 4\text{V}$ , whilst Fig. 6 shows that the IDZ approximation is most accurate for inputs in the range  $v_{\min}$  to  $v_{\max}$  selected above. In fact, the closed-loop response is not particularly sensitive to these values since the design poles are selected to avoid hitting the constraints anyway (see below).

A simulation study into the effectiveness of different control approaches, including e.g. PI, PIP, SDP and fuzzy logic algorithms, all with and without the IDZ control element, is beyond the scope of this article and will be reported in future work. However, with a focus on illustrating the veracity of the novel SDP model identification process proposed above, Fig. 7 compares the closed-loop simulation response with experimental data from the BROKK system, for PIP-IDZ control of J2.

The controller is based on closed-loop poles on the complex  $z$ -plane of  $(0.9 + 0.05i, 0.9 - 0.05i, 0, 0)$ , initially obtained using linear quadratic design methods, which yields  $f_0 = 0.1261$ ,  $g_1 = 0.12$ ,  $g_2 = 0.1261$  and  $k_I = 0.0061$ . Fig. 7 shows that the PIP-IDZ algorithm yields a smooth, relatively fast closed-loop response, comparable to earlier research using the more complex nonlinear pole assignment approach (Taylor and Robertson, 2013). Similar results have been obtained for other joints and for resolved motion. Of particular significance to the present article, however, Fig. 7 also shows that the identified SDP model adequately represents the experimental data.

## 7. CONCLUSIONS

The article has identified SDP models for the manipulator joints of a BROKK-based nuclear decommissioning robot. Recent results linking regret-regression and state-space modelling have been exploited for the parametric stage of this analysis. Such methods have potential value for short experiments with noisy (angular velocity) data. In contrast to earlier research, the SDP model structure is obtained directly from a mechanistic interpretation of the preliminary RIV estimation results. The SDP models obtained in this manner facilitate use of an IDZ method for control system design. This is rather simpler to implement than an earlier SDP approach and has the advantage of combining the input signal calibration, system identification and control system design steps, all based on a relatively small data-set. This allows for rapid application to each joint and straightforward recalibration when the dynamic

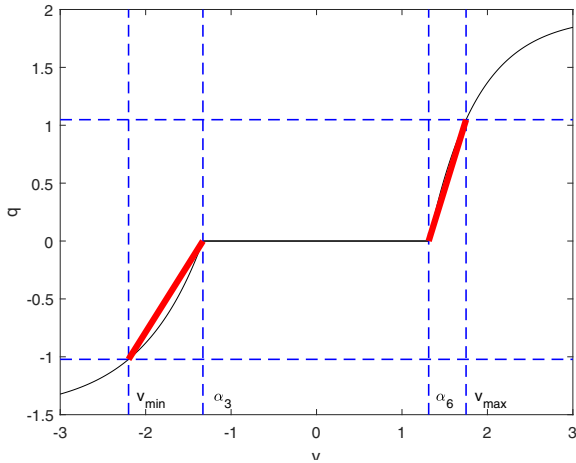


Fig. 6. IDZ approximation, showing angular velocity  $q_k$  (degrees/sample,  $\Delta t = 0.05s$ ) against input (i.e. steady state voltage to NI-CFP,  $v_\infty$ ), showing  $b_\tau \{\chi_k\} \times v_\infty / \Delta t$  (thin solid trace) and linearised model (thick). The estimated dead-zone and chosen velocity saturation limits are highlighted (dashed).

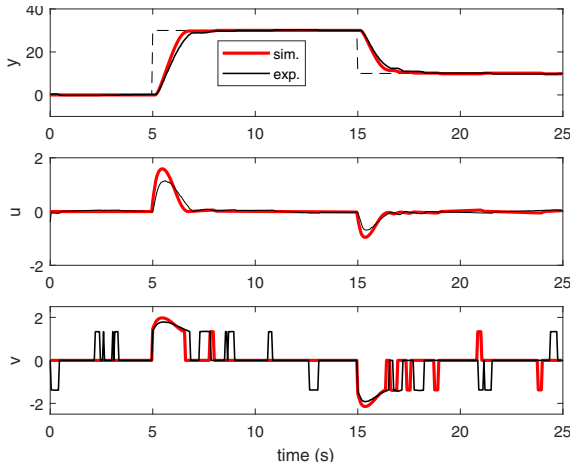


Fig. 7. PIP-IDZ control, showing the command (dashed), experimental data (thin solid trace) and SDP simulation (thick). Joint angle  $y_k$  (degrees), PIP control input  $u_k$  and voltage to the NI-CFP  $v_k$  are shown from top to bottom, all plotted against time (s).

characteristics have changed due to age and use, or after the installation of replacement parts.

## REFERENCES

Clairon, Q., Wilson, E.D., Henderson, R., and Taylor, C.J. (2017). Adaptive biomedical treatment and robust control. In *20th IFAC Triennial World Congress*. Toulouse.

Fortgang, J.D., George, L.E., and Book, W.J. (2002). Practical implementation of a dead zone inverse on a hydraulic wrist. In *ASME International Mechanical Engineering Congress and Exposition*. New Orleans.

Gautier, M., Janot, A., and Vandanjon, P.O. (2013). A new closed-loop output error method for parameter identification of robot dynamics. *IEEE Transactions on Control System Technology*, 21, 428–444.

Gautier, M. and Poignet, P. (2001). Extended Kalman filtering and weighted LS dynamic identification of robot. *Control Engineering Practice*, 9, 1361–1372.

Hashemi, S., Abbas, H., and Werner, H. (2012). Low-complexity LPV modeling and control of a robotic manipulator. *Control Engineering Practice*, 12, 248–257.

Henderson, R., Ansell, P., and Alsibani, D. (2010). Regret-regression for optimal dynamic treatment regimes. *Biometrics*, 66, 1192–1201.

Janot, A., Vandanjon, P.O., and Gautier, M. (2014). An instrumental variable approach for rigid industrial robots identification. *Control Eng. Practice*, 25, 85–101.

Janot, A., Young, P.C., and Gautier, M. (2017). Identification and control of electro-mechanical systems using state-dependent parameter estimation. *International Journal of Control*, 90, 643–660.

Kent, D., Saldanha, C., and Chernova, S. (2017). A comparison of remote robot teleoperation interfaces for general object manipulation. In *ACM/IEEE International Conference on Human-Robot Interaction*. Vienna.

Marturi, N., Rastegarpanah, A., Takahashi, C., Adjigble, M., Stolkin, R., Zurek, S., Kopicki, M., Talha, M., Kuo, J.A., and Bekiroglu, Y. (2016). Towards advanced robotic manipulation for nuclear decommissioning: A pilot study on tele-operation and autonomy. In *IEEE Robotics & Automation for Humanitarian App*. Kollam.

Montazeri, A., West, C., Monk, S., and Taylor, C.J. (2017). Dynamic modeling and parameter estimation of a hydraulic robot manipulator using a multi-objective genetic algorithm. *International J. Control*, 90, 661–683.

Olsen, M.M., Swevers, J., and Verdonck, W. (2001). ML identification of a dynamic robot model: Implementation issues. *Int. J. Robotics Research*, 21, 9–96.

Robertson, D., Taylor, C.J., and Lokuciewski, C. (2012). State-dependent system identification for control of a hydraulically-actuated nuclear decommissioning robot. In *16th IFAC Symp. System Identification*. Brussels.

Sirouspour, M.R. and Salcudean, S.E. (2001). Nonlinear control of hydraulic robots. *IEEE Transactions on Robotics and Automation*, 17, 173–182.

Taylor, C.J., Chotai, A., and Burnham, K.J. (2011). Controllable forms for stabilising pole assignment design of generalised bilinear systems. *Elect. Letters*, 47, 437–439.

Taylor, C.J., Pedregal, D.J., Young, P.C., and Tych, W. (2007a). Environmental time series analysis and forecasting with the Captain Toolbox. *Environmental Modelling and Software*, 22, 797–814.

Taylor, C.J. and Robertson, D. (2013). State-dependent control of a hydraulically-actuated nuclear decommissioning robot. *Control Eng. Practice*, 21, 1716–1725.

Taylor, C.J., Shaban, E.M., Stables, M.A., and Ako, S. (2007b). PIP control applications of SDP models. *IMechE Proceedings Part I*, 221, 1019–1032.

Taylor, C.J., Young, P.C., and Chotai, A. (2013). *True Digital Control: Statistical Modelling and Non-Minimal State Space Design*. John Wiley and Sons.

Wernholt, E. and Gunnarsson, S. (2008). Estimation of nonlinear effects in frequency domain identification of industrial robots. *IEEE Transactions on Instrumentation and Measurement*, 57, 856–863.

West, C., Montazeri, A., Monk, S.D., Duda, D., and Taylor, C.J. (2017). A new approach to improve the parameter estimation accuracy in robotic manipulators. In *26th IEEE Robot and Human Int. Comm*. Lisbon.

Young, P.C. (2011). *Recursive Estimation and Time Series Analysis*. Springer.